

Discrete Contrastive Diffusion for Cross-Modal and Conditional Generation

Ye Zhu
Illinois Institute of Technology

Yu Wu
Princeton University

Kyle Olszewski
Snap Inc.

Jian Ren
Snap Inc.

Sergey Tulyakov
Snap Inc.

Yan Yan
Illinois Institute of Technology

Abstract

Diffusion probabilistic models (DPMs) have become a popular approach to conditional generation, due to their promising results and support for cross-modal synthesis. A key desideratum in conditional synthesis is to achieve high correspondence between the conditioning input and generated output. Most existing methods learn such relationships implicitly, by incorporating the prior into the variational lower bound. In this work, we take a different route—we enhance input-output connections by maximizing their mutual information using contrastive learning. To this end, we introduce a *Conditional Discrete Contrastive Diffusion (CDCD)* loss and design two contrastive diffusion mechanisms to effectively incorporate it into the denoising process. We formulate *CDCD* by connecting it with the conventional variational objectives. We demonstrate the efficacy of our approach in evaluations with three diverse, multimodal conditional synthesis tasks: dance-to-music generation, text-to-image synthesis, and class-conditioned image synthesis. On each, we achieve state-of-the-art or higher synthesis quality and improve the input-output correspondence. Furthermore, the proposed approach improves the convergence of diffusion models, reducing the number of required diffusion steps by more than 35% on two benchmarks, significantly increasing the inference speed.¹

1 Introduction

Generative tasks that seek to synthesize data in different modalities, such as audio and images, have attracted much attention. The recently explored diffusion probabilistic models (DPMs) [64] have served as a powerful generative backbone that achieves promising results in both unconditional and conditional generation [42, 51, 45, 32, 52, 16, 33, 35, 28]. Compared to the unconditional case, conditional generation is usually applied in more concrete and practical cross-modality scenarios, *e.g.* video-based music generation [17, 90, 23] and text-based image generation [28, 59, 57, 46, 61, 59]. Most existing DPM-based conditional synthesis works [28, 16] learn the connection between the conditioning and the generated data implicitly by adding a prior to the variational lower bound [64]. While such approaches still feature high generation fidelity, the correspondence between the conditioning and the synthesized data can sometimes get lost, as illustrated in the right column in Fig. 1. To this end, we aim to explicitly enhance the input-output correspondence via their maximized mutual information under the diffusion generative framework for conditional settings in this paper. Several examples of our synthesized audio and image results are given in Fig. 1.

Inspired by the success of contrastive representation learning [53, 6, 29, 12], we propose to improve the desired connections via the maximization of mutual information between the input conditioning

¹Codes and samples at <https://github.com/L-YeZhu/CDCD>.

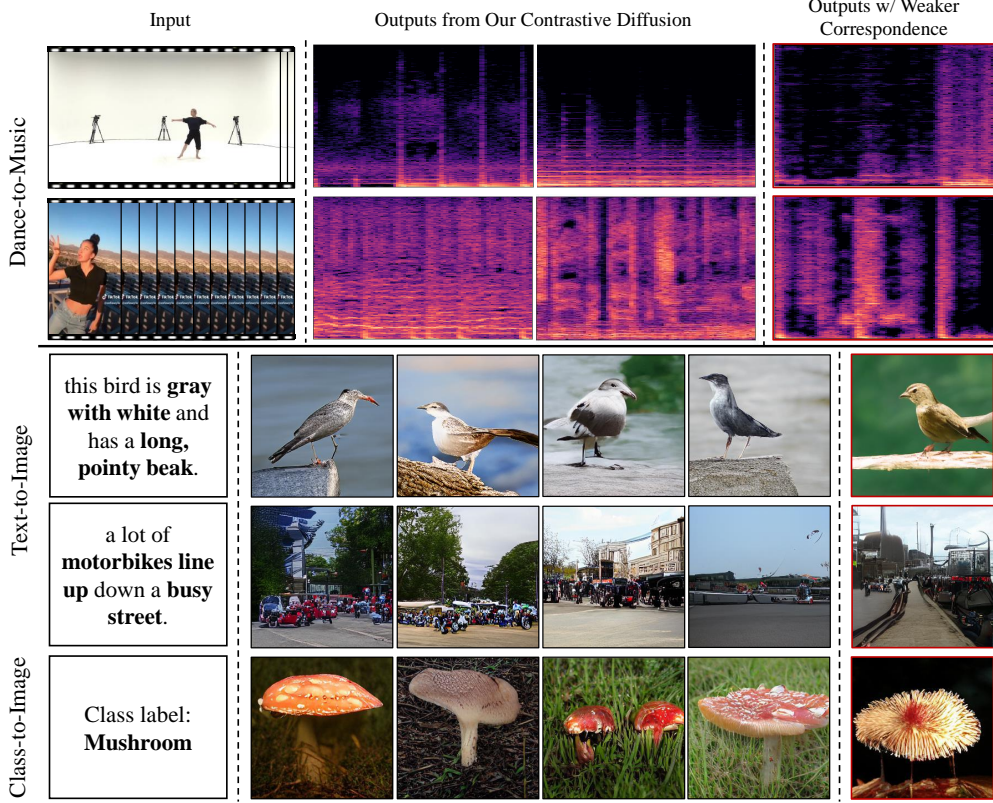


Figure 1: Examples of the input (left column) and synthesized output (middle column) from our contrastive diffusion model for video-to-music (Rows 1-2), text-to-image (Rows 3-4), and class-conditioned (Row 5) generation experiments on five datasets. The right column shows some synthesized data with reasonable quality but weaker correspondence to the input from existing methods [90, 28]. Consider: in Row 3, the bird is *yellow*, not *gray-white*, and has no *pointy beak*; in Row 4, *motorbikes* are hardly visible; in Row 5, the object is a *flower* that is just shaped like a *mushroom*.

and output data. Typical contrastive representation learning methods [53, 6, 66] seek to learn an embedding z of raw data x based on the assumption that a properly encoded z benefits the ability of a generative model p to reconstruct the raw data given z as prior. This idea can be achieved via optimization of the density ratio $\frac{p(x|z)}{p(x)}$ [53] as an entirety, without explicitly modeling the actual generative model p . As shown in previous literature [67, 7], the direct optimization of mutual information via generative models is a challenging problem to implement and train. To this end, we reformulate the optimization problem for the desired conditional generative tasks via DPMs by analogy to the above embedding and raw data with our conditioning input and synthesized output. Specifically, we introduce a *Conditional Discrete Contrastive Diffusion (CDCD)* loss, and design two contrastive diffusion mechanisms - *step-wise parallel diffusion* that invokes multiple parallel diffusion processes during contrastive learning, and *sample-wise auxiliary diffusion*, which maintains one principal diffusion process, to effectively incorporate the *CDCD* loss into the denoising process. We show that with the proposed contrastive diffusion method, we can not only effectively train so as to maximize the desired mutual information by connecting the *CDCD* loss with the conventional variational objective function, but also to directly optimize the generative network p . The optimized *CDCD* loss encourages faster convergence of a DPM model with fewer diffusion steps. We further present our *intra-* and *inter-negative* sampling methods by providing internally disordered and instance-level negative samples, respectively.

Various generative settings, frameworks, and applications can benefit from our contrastive diffusion approach, *e.g.* joint or separate training of conditioning encoders, continuous or discrete conditioning inputs, and diverse input-output modalities as detailed in Sec. 4. With this approach, we achieve results comparable or superior to state-of-the-art on three conditional synthesis tasks: dance-to-music

(datasets: AIST++ [76, 47], TikTok Dance-Music [90]), text-to-image (datasets: CUB200 [78], MSCOCO [48]) and class-conditioned image synthesis (dataset: ImageNet [62]). Our experimental findings suggest three key take-home messages: ① Improving the input-output connections via maximized mutual information is indeed beneficial for their correspondence and the general fidelity of the results (see Fig. 1 and our project page). ② Both *step-wise parallel diffusion* with *intra*-negative samples and *sample-wise auxiliary diffusion* with *inter*-negative samples show state-of-the-art scores in our evaluations. The former is more beneficial for capturing the intra-sample correlations, *e.g.* musical rhythms in dance-to-music, while the latter improves the instance-level performance for image synthesis. ③ With maximized mutual information, our conditional contrastive diffusion models *converge in substantially fewer diffusion steps* compared to vanilla DPMs, while maintaining the same or even superior performance (approximately **35%** fewer steps for dance-to-music generation and **40%** fewer for text-to-image synthesis), thus significantly increasing inference speed after training.

2 Background

Diffusion Probabilistic Models. DPMs [64] are a class of generative models that learn to convert a simple Gaussian distribution into a data distribution. This process consists of a forward *diffusion* process and a reverse *denoising* process, each consisting of a sequence of T steps that act as a Markov chain. During forward diffusion, an input data sample x_0 is gradually “corrupted” at each step t by adding Gaussian noise to the output of step $t - 1$. The reverse denoising process, seeks to convert the noisy latent variable x_T into the original data sample x_0 by removing the noise added during diffusion. The stationary distribution for the final latent variable x_T is typically assumed to be a normal distribution, $p(x_T) = \mathcal{N}(x_T|0, \mathbf{I})$.

An extension of this approach replaces the continuous state with a discrete one [65, 34, 4], in which the latent variables $x_{1:T}$ typically take the form of one-hot vectors with K categories. The diffusion process can then be parameterized using a categorical transition matrix defined as $q(x_t|x_{t-1}) = \text{Cat}(x_t; p = x_{t-1}Q_t)$, where $[Q_t]_{ij} = q(x_t = j|x_{t-1} = i)$. The reverse process $p_\theta(x_t|x_{t-1})$ can also factorized as conditionally independent over the discrete sequences [4].

In both the continuous and discrete state formulations of DPMs [70, 71, 41, 69, 36, 77], the denoising process p_θ can be optimized by the KL divergence between q and p_θ in closed forms [68, 52, 32, 34, 4] via the variational bound on the negative log-likelihood:

$$\mathcal{L}_{\text{vb}} = \mathbb{E}_q \left[\underbrace{D_{\text{KL}}(q(x_T|x_0)||p(x_T))}_{\mathcal{L}_T} + \sum_{t>1} \underbrace{D_{\text{KL}}(q(x_{t-1}|x_t, x_0)||p_\theta(x_{t-1}|x_t))}_{\mathcal{L}_{t-1}} - \underbrace{\log p_\theta(x_0|x_1)}_{\mathcal{L}_0} \right]. \quad (1)$$

Existing conditional generation works via DPMs [28, 16] usually learn the implicit relationship between the conditioning c and the synthesized data x_0 by directly adding the c as the prior in Eq. (1). The DPMs with discrete state space provide more controls on the data corruption and denoising compared to its continuous counterpart [4, 28], which benefits the conditional generation with more flexibility for practical downstream operations such as editing and interactive synthesis [75, 13, 84]. We hence employ contrastive diffusion using a discrete state space in this work.

Vector-Quantized Representations for Conditional Generation. Vector quantization is a classical technique in which a high-dimensional space is represented using a discrete number of vectors, which has proven effective in tasks ranging from data compression to density estimation [27, 26]. More recently, Vector-Quantized (VQ) deep learning models have employed this technique to allow for compact and discrete representations of images and other data that allow for high-resolution image synthesis and the conditional generation of images and audio [54, 60, 22, 15].

Using this approach, we employ an encoder-decoder framework in which we learn a “codebook” containing a fixed number of vectors used to represent the input data. The encoder transforms the input x into a set of vectors that are each mapped to the closest corresponding vector in the codebook, while the decoder uses the set of quantized vectors z to reconstruct the input data, producing x' . By manipulating the quantized representation based on conditioning information, *e.g.* using a transformer as in our approach, we can generate data in the target domain that corresponds to the conditioning input. As we employ a diffusion model which generates the conditioned target data over several steps, we refer to z , the latent quantized representation of x , as z_0 below to distinguish it from the latent representation at prior stages in the denoising process. As our approach is flexible enough to be employed with various input and output modalities, the exact underlying VQ model we use depends

on the target data domain. For audio synthesis, we employ a fine-tuned Jukebox [15] model, while for image generation, we employ VQ-GAN [22]. Please see Sec. 4 for further details.

Contrastive Representation Learning. Contrastive learning uses loss functions designed to make neural networks learn to understand and represent the specific similarities and differences between elements in the training data without labels explicitly defining such features. An effective approach to this is to employ *positive* pairs of data points (*e.g.*, images depicting the same category of object) and *negative* pairs (*e.g.*, images of different types of objects) to encourage the network to learn representations of these data points that are similar for positive pairs and different for negative pairs. This approach has been successfully applied in learning representations of high-dimensional data [53, 6, 29, 66, 12]. Many such works seek to maximize the mutual information between the original data x and its learned representation z under the framework of likelihood-free inference [53, 66, 19]. The above problem can be formulated as maximizing a density ratio $\frac{p(x|z)}{p(x)}$ that preserves the mutual information between the raw data x and learned representation z .

To achieve this, existing contrastive methods [53, 19, 29, 86] typically adopt a neural network to directly model the ratio as an entirety and avoid explicitly considering the actual generative model $p(x|z)$, which has proven to be a more challenging problem [67, 7]. In contrast, we show that by formulating the conventional contrastive representation learning problem under the generative setting, the properties of DPMs enable us to directly optimize the model p in this work, which can be interpreted as the optimal version of the density ratio [53].

3 Method

Here we outline our approach to cross-modal and conditional generation using our proposed discrete contrastive diffusion approach, which is depicted in Fig. 2. In Sec. 3.1, we formulate our Conditional Discrete Contrastive Diffusion loss in detail, and demonstrate how it helps to maximize the mutual information between the conditioning and generated discrete data representations. Sec. 3.2 defines two specific mechanisms for applying this loss within a diffusion model training framework, *sample-wise* and *step-wise*. In Sec. 3.3, we detail techniques for constructing negative samples designed to improve the overall quality and coherence of the generated sequences.

3.1 Conditional Discrete Contrastive Diffusion Loss

Given the data pair (c, x) , where c is the conditioning information from a given input modality (*e.g.*, videos, text, or a class label), our objective is to generate a data sample x in the target modality (*e.g.*, audio or images) corresponding to c . We employ an encoder-decoder framework that uses a vector-quantized (VQ) representation as its discrete state space. Thus, our diffusion process operates on the encoded latent representation z_0 of x . The denoising process recovers the latent representation z_0 given the conditioning c that can be decoded to obtain the reconstruction x' .

We seek to enhance the connection between c and the generated data z_0 by maximizing their mutual information, defined as $I(z_0; c) = \sum_{z_0} p_\theta(z_0, c) \log \frac{p_\theta(z_0|c)}{p_\theta(z_0)}$. We introduce a set of negative VQ sequences $Z' = \{z^1, z^2, \dots, z^N\}$, encoded from N negative samples $X' = \{x^1, x^2, \dots, x^N\}$, and define $f(z_0, c) = \frac{p_\theta(z_0|c)}{p_\theta(z_0)}$. Our proposed Conditional Discrete Contrastive Diffusion (CDCD) loss is:

$$\mathcal{L}_{\text{CDCD}} = -\mathbb{E} \left[\log \frac{f(z_0, c)}{f(z_0, c) + \sum_{z^j \in Z'} f(z_0^j, c)} \right]. \quad (2)$$

The proposed *CDCD* loss is similar to the categorical cross-entropy loss for classifying the positive sample as in [53], where our conditioning c and the generated data z_0 corresponds to the original learned representation and raw data, and optimization of this loss leads to maximization of $I(z_0; c)$. However, the loss in [53] models the density ratio $f(z_0, c)$ as an entirety. In our case, we demonstrate that the DPMs properties [64, 32, 4] enable us to directly optimize the actual distribution p_θ within the diffusion process for the desired conditional generation tasks. Specifically, we show the connections between the proposed *CDCD* loss and the conventional variational loss \mathcal{L}_{vb} (see Eq. (1)) in Sec. 3.2, and thus how it contributes to efficient DPM learning. Additionally, we can derive the lower bound for the mutual information as $I(z_0; c) \geq \log(N) - \mathcal{L}_{\text{CDCD}}$ (see project page for details), which

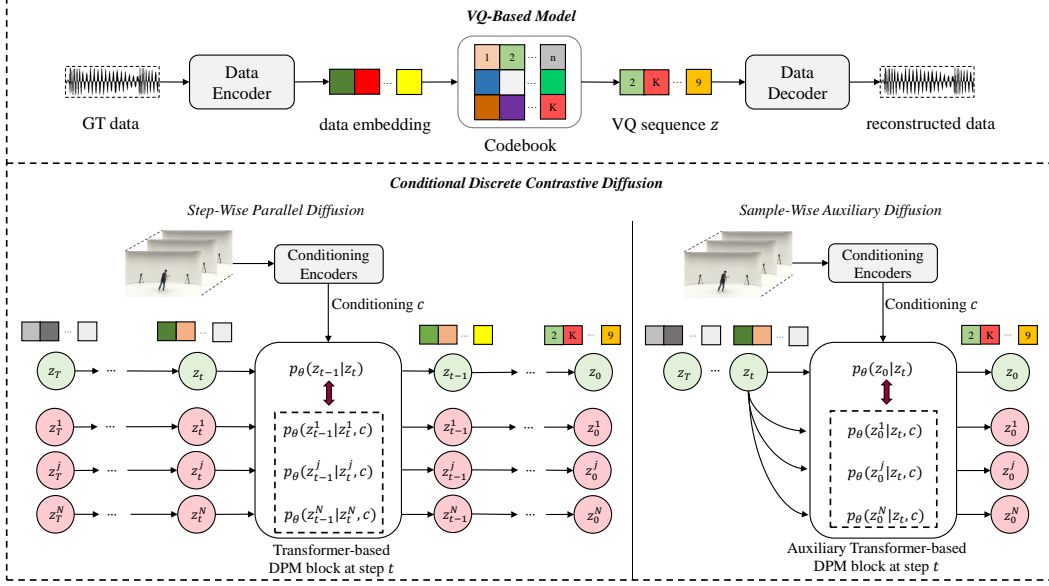


Figure 2: **Overview of the proposed pipeline.** Our framework includes two major components: a VQ-based encoder-decoder model (top) and a conditioned discrete contrastive diffusion model (bottom). In the contrastive diffusion stage, we illustrate our proposed step-wise parallel diffusion (bottom left) and sample-wise auxiliary diffusion (bottom right). The variables in green denote those from the principal diffusion process, while the variables in red represent the diffusion invoked by negative samples. Here we show audio generation from video input, but demonstrate that this approach extends to radically different modalities, e.g. text-to-image.

indicates that a larger number of negative samples increases the lower bound. These two factors allow for *faster* convergence of a DPM with *fewer* diffusion steps.

3.2 Parallel and Auxiliary Diffusion Process

The *CDCD* loss in Eq. (2) considers the mutual information between c and z_0 in a general way, without specifying the intermediate diffusion steps. We propose and analyze two contrastive diffusion mechanisms to efficiently incorporate this loss into DPM learning, and demonstrate that we can directly optimize the generative model p_θ in the diffusion process. We present our *step-wise parallel diffusion* and the *sample-wise auxiliary diffusion* mechanisms, which are distinguished by the specific operations applied for the intermediate negative latent variables $z_{1:T}^j$ for each negative sample x^j .

Step-Wise Parallel Diffusion. This mechanism not only focuses on the mutual information between c and z_0 , but also takes the intermediate negative latent variables $z_{1:T}^j$ into account by explicitly invoking the complete diffusion process for each negative sample $z^j \in Z'$. As illustrated in Fig. 2 (bottom left), we initiate $N + 1$ parallel diffusion processes, among which N are invoked by negative samples. For each negative sample $x^j \in X'$, we explicitly compute its negative latent discrete variables $z_{0:T}^j$. In this case, Eq. (2) is as follows (see supplement for the detailed derivation):

$$\mathcal{L}_{\text{CDCD-Step}} \approx \mathbb{E}_Z \log \left[1 + \frac{p_\theta(z_{0:T})}{p_\theta(z_{0:T}|c)} N \mathbb{E}_{Z'} \left[\frac{p_\theta(z_{0:T}^j|c)}{p_\theta(z_{0:T}^j)} \right] \right] \approx \mathcal{L}_{\text{vb}}(z) - \sum_{z^j \in Z'} \mathcal{L}_{\text{vb}}(z^j, c). \quad (3)$$

The equation above factorizes the proposed *CDCD* loss using the step-wise parallel diffusion mechanism into two terms, where the first term corresponds to the original variational bound \mathcal{L}_{vb} , and the second term can be interpreted as the negative sum of variational bounds induced by the negative samples and the provided conditioning c .

Sample-Wise Auxiliary Diffusion. Alternatively, our *sample-wise auxiliary diffusion* mechanism maintains one principal diffusion process, as in traditional diffusion training, shown in Fig. 2 (bottom right). It contrasts the intermediate *positive* latent variables $z_{1:T}$ with the negative sample $z_0^j \in Z$. In

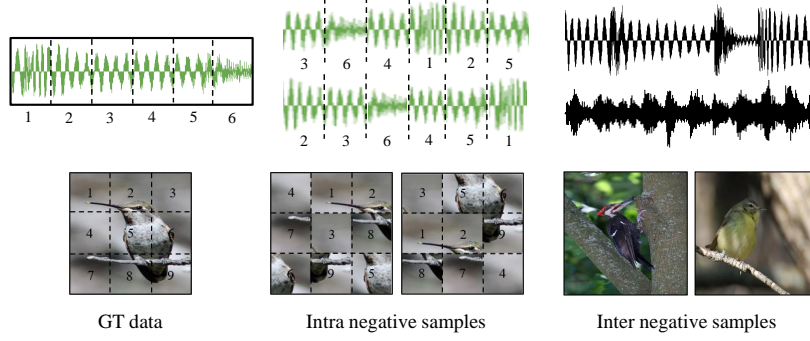


Figure 3: Illustration of *intra*- and *inter*-negative sampling for music and image data.

this case, we can write the *CDCD* loss from Eq. (2) as (see supplement for details):

$$\mathcal{L}_{\text{CDCD-Sample}} \approx \mathbb{E}_q[-\log p_\theta(z_0|z_t)] - \sum_{z^j \in Z'} \mathbb{E}_q[-\log p_\theta(z_0^j|z_t, c)]. \quad (4)$$

As with the step-wise loss, the *CDCD-Sample* loss includes two terms. The first refers to sampling directly from the positive z_0 at an arbitrary timestep t . The second sums the same auxiliary loss from negative samples z_0^j . This marginalization operation is based on the property of Markov chain as in previous discrete DPMs [4, 28], which imposes direct supervision from the sample data. The first term is similar to the auxiliary denoising objective in [4, 28].

Both contrastive diffusion mechanisms enable us to effectively incorporate the *CDCD* loss into our DPM learning process by directly optimizing the actual denoising generative network p_θ .

Final Loss Function. The final loss function for our contrastive diffusion training process is:

$$\mathcal{L} = \mathcal{L}_{\text{vb}} + \lambda \mathcal{L}_{\text{CDCD}}, \quad (5)$$

where $\mathcal{L}_{\text{CDCD}}$ refers to either the step-wise parallel diffusion or sample-wise auxiliary diffusion loss. Empirically, we can omit the first term in Eq. (3), or directly optimize $\mathcal{L}_{\text{CDCD-Step}}$, in which the standard \mathcal{L}_{vb} is already included. The detailed training algorithm is explained in the supplement.

3.3 Intra- and Inter-Negative Sampling

Previous contrastive works construct negative samples using techniques such as image augmentation [12, 29] or spatially adjacent image patches [53]. In this work, we categorize our sampling methods into *intra*- and *inter*-negative samplings as in Fig. 3. For the *intra*-sample negative sampling, we construct X' based on the given original x . This bears resemblance to the patch-based technique in the image domain [53]. As for the audio data, we first divide the original audio waveform into multiple chunks, and randomly shuffle their ordering. For the *inter*-sample negative sampling, X' consists of instance-level negative samples x' that differ from the given data pair (c, x) . In practice, we define negative samples x' to be music sequences with different musical genres from x in the music generation task, while x' denotes images other than x in the image synthesis task.

Based on our proposed contrastive diffusion modes and negative sampling methods, there are four possible contrastive settings: step-wise parallel diffusion with either intra- or inter-negative sampling (denoted as *Step-Intra* and *Step-Inter*), or sample-wise auxiliary diffusion with either intra- or inter-negative sampling (denoted as *Sample-Intra* and *Sample-Inter*). Intuitively, we argue that *Step-Intra* and *Sample-Inter* settings are more reasonable compared to *Step-Inter* and *Sample-Intra* because of the consistency between the diffusion data corruption process and the way to construct negative samples. Specifically, the data corruption process in the discrete DPMs includes sampling and replacing certain tokens with some random or mask tokens at each diffusion step [4, 28], which is a chunk-level operation within a given data sequence similar to the ways we construct *intra*-negative samples by shuffling the chunk-level orders. In contrast, the *sample-wise auxiliary diffusion* seeks to provide sample-level supervision, which is consistent with our inter-negative sampling method.

In the interest of clarity and concision, we only present the experimental results for *Step-Intra* and *Sample-Inter* settings in Sec. 4 of our main paper. The complete results obtained with other contrastive settings and more detailed analysis are included in the supplement.

Table 1: Quantitative evaluation results for the dance-to-music task on the AIST++ dataset. This table shows the best performance scores we obtain for different contrastive diffusion steps. We report the mean and standard deviations of our contrastive diffusion for three inference tests.

Musical features	Rhythms	Rhythms	Genre	Coherence	Quality
Metrics	Coverage \uparrow	Hit \uparrow	Accuracy \uparrow	MOS \uparrow	MOS \uparrow
GT Music	100	100	88.5	4.7	4.8
Foley [23]	74.1	69.4	8.1	2.9	-
Dance2Music [1]	83.5	82.4	7.0	3.0	-
CMT [17]	85.5	83.5	11.6	3.0	-
D2M-GAN [90]	88.2	84.7	24.4	3.3	3.4
Ours Vanilla	89.0 \pm 1.1	83.8 \pm 1.5	25.3 \pm 0.8	3.3	3.6
Ours Step-Intra	93.9 \pm 1.2	90.7 \pm 1.5	25.8 \pm 0.6	3.6	3.5
Ours Sample-Inter	91.8 \pm 1.6	86.9 \pm 1.4	27.2 \pm 0.5	3.6	3.6

Table 2: Quantitative evaluation results for the dance-to-music task on the TikTok dataset. We set the default number of diffusion steps to be 80.

Methods	Beats Coverage/Hit \uparrow
D2M-GAN [90]	88.4/ 82.3
Ours Vanilla	88.7/ 81.4
Ours Step-Intra	91.8/ 86.3
Ours Sample-Inter	90.1/ 85.5

4 Experiments

We conduct experiments on three conditional generation tasks: dance-to-music generation, text-to-image synthesis, and class-conditioned image synthesis. For the dance-to-music task, we seek to generate audio waveforms for complex music from human motion and dance video frames. For the text-to-image task, the objective is to generate images from given textual descriptions.

4.1 Dance-to-Music Generation

Dataset. We use the AIST++ [47] dataset and the TikTok Dance-Music dataset [90] for the dance-to-music experiments. AIST++ is a subset of the AIST dataset [76], which contains 1020 dance videos and 60 songs performed by professional dancers and filmed in clean studio environment settings without occlusions. AIST++ provide human motion data in the form of SMPL [49] parameters and body keypoints, and includes the annotations for different genres and choreography styles. The TikTok Dance-Music dataset includes 445 dance videos collected from the social media platform. The 2D skeleton data extracted with OpenPose [10, 9] is used as the motion representation. We adopt the official cross-modality splits without overlapping music songs for both datasets.

Implementations. The sampling rate for all audio signals is 22.5 kHz in our experiments. We use 2-second music samples as in [90] for the main experiments. We fine-tuned the pre-trained Jukebox [15] for our Music VQ-VAE model. For the motion encoder, we deploy a backbone stacked with convolutional layers and residual blocks. For the visual encoder, we extract I3D features [11] using a model pre-trained on Kinetics [39] as the visual conditioning. The motion and visual encoder outputs are concatenated to form the final continuous conditioning input to our contrastive diffusion model. For the contrastive diffusion model, we adopt a transformer-based backbone to learn the denoising network p_θ . It includes 19 transformer blocks, with each block consisting of full attention, cross attention and feed forward modules, and a channel size of 1024 for each block. We set the initial weight for the contrastive loss as $\lambda = 5e - 5$. The number N of intra- and inter-negative samples for each GT music sample is 10. The visual encoder, motion encoder, and the contrastive diffusion model are jointly optimized. More implementation details are provided in the supplement.

Evaluations. The evaluation of synthesized music measures both the conditioning-output correspondence and the general synthesis quality using the metrics introduced in [90]. Specifically, the metrics include the beats coverage score, the beats hit scores, the genre accuracy score, and two subjective evaluation tests with Mean Opinion Scores (MOS) for the musical coherence and general quality. Among these metrics, the beats scores emphasize the intra-sample properties, since they calculate the second-level audio onset strength within musical chunks [20], while the genre accuracy focuses on the instance-level musical attributes of music styles. Detailed explanations of the above metrics can be found in [90]. We compare against multiple dance-to-music generation works: Foley [23], Dance2Music [1], CMT [17], and D2M-GAN [90]. The first three models rely on symbolic discrete MIDI musical representations, while the last one also uses a VQ musical representation. The major difference between the symbolic MIDI and discrete VQ musical representations lies within the fact that the MIDI is pre-defined for each instrument, while the VQ is learning-based. The latter thus enables complex and free music synthesis appropriate for scenarios like dance videos [90].

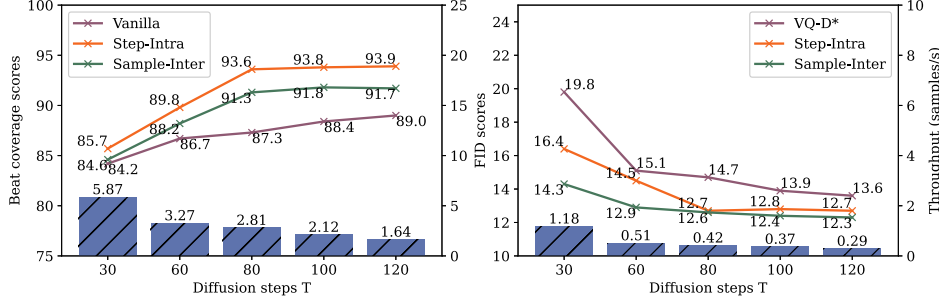


Figure 4: Convergence analysis in terms of diffusion steps for the dance-to-music task on AIST++ dataset (left) and the text-to-image task on CUB200 dataset (right). We observe that our contrastive diffusion models converge at around 80 steps and 60 steps, resulting 35% steps and 40% steps less compared to the vanilla models that converge at 120 steps and 100 steps, while maintaining superior performance, respectively. We use the same number of steps for training and inference.

Results and Discussion. The quantitative experimental results are shown in Tab. 1 and Tab. 2. Our proposed methods achieve better performance than the competing methods even with vanilla version without contrastive mechanisms. Furthermore, we find that the *Step-Intra* setting is more helpful in increasing the beats scores, while the *Sample-Inter* setting yields more improvements for the genre accuracy scores. We believe this is due to the evaluation methods of different metrics. The beats scores measure the chunk-level (*i.e.*, the audio onset strength [20]) consistency between the GT and synthesized music samples [90], while the genre scores consider the overall musical attributes of each sample sequence in instance level. This finding is consistent with our assumptions in Sec. 3.3.

Convergence Analysis. We also analyze the impact of the proposed contrastive diffusion on model convergence in terms of diffusion steps. The number of diffusion steps is a significant hyper-parameter for DPMs [64, 52, 4, 28, 41] that directly influences the inference time and synthesis quality. Previous works have shown that a larger number of diffusion steps usually lead to better model performance, but longer inference times [41, 28]. We demonstrate that, with the improved mutual information via the proposed contrastive diffusion method, we can greatly reduce the number of steps needed for the diffusion models. As shown in Fig. 4 (left), we observe that the beats scores reach a stable level at approximately 80 steps, $\sim 35\%$ less than the vanilla DPM that converges in ~ 120 steps. More ablation studies and analysis on the dance-to-music task can be found in the supplement.

4.2 Conditional Image Synthesis

Dataset. We conduct text-to-image synthesis on CUB200 [78] and MSCOCO datasets [48]. The CUB200 dataset contains images of 200 bird species. The training and testing splits include 8855 and 2933 images, respectively. Each image has 10 corresponding text descriptions. The MSCOCO dataset contains 82k images for training and 40k images for testing. Each image has 5 text descriptions.

Implementation. For the text-to-image generation task, we adopt VQ-GAN [22] as the discrete encoder and decoder. VQ-GAN converts a 256×256 resolution image to 32×32 discrete tokens. For the textual conditioning, we utilize the pre-trained CLIP [57] model to encode the given textual descriptions. The denoising diffusion model p_θ has 18 transformer blocks and a channel size of 192, which has similar model scale to the small version of VQ-Diffusion [28]. We use $\lambda = 5e - 5$ as the contrastive loss weight. Other detailed parameters can be found in the supplement.

Evaluations. We adopt two evaluation metrics to assess the obtained results: the classic FID score [31] as the general measurement for image quality, and the CLIPScore [30] to evaluate the correspondence between the given textual caption and the synthesized image. We compare against text-to-image generation methods including StackGAN [87], StackGAN++ [88], SEGAN [72], AttnGAN [83], DM-GAN [89], DF-GAN [73], DAE-GAN [61], DALLE [59], and VQ-Diffusion [28]. Specifically, VQ-Diffusion [28] also adopts the discrete diffusion generative backbone, which can be considered as the vanilla version without contrastive mechanisms.

Results and Discussion. The quantitative results are represented in Tab. 3. We observe that our contrastive diffusion approaches achieve state-of-the-art performance for both FID and CLIPScores,

Table 3: FID and CLIPScore for text-to-image synthesis on CUB-200 and MSCOCO datasets. The VQ-D model with * shows the results we reproduced by training using the original code, which can be considered as our baseline. We show the results obtained with default 80 diffusion steps in both training and inference.

Datasets Metrics	CUB-200		MSCOCO	
	FID ↓	CLIPScore ↑	FID ↓	CLIPScore ↑
StackGAN [87]	51.89	-	74.05	-
StackGAN++ [88]	15.30	-	81.59	-
SEGAN [72]	18.17	-	32.28	-
AttnGAN [83]	23.98	-	35.49	65.66
DM-GAN [89]	16.09	-	32.64	65.45
DF-GAN [73]	14.81	-	21.42	66.42
DAE-GAN [61]	15.19	-	28.12	-
DALLE [59]	56.10	74.66	27.50	-
VQ-D (T=100) [28]	12.97	-	30.17	-
VQ-D* (T=80)	14.61	74.96	36.45	65.53
Ours Step-Intra (T=80)	12.73	75.32	32.25	66.22
Ours Sample-Inter (T=80)	12.61	75.50	28.76	66.79

Table 4: FID scores for class-conditioned image synthesis on ImageNet 256 × 256. Our model follows the *Sample-Inter* contrastive setting with 80 diffusion steps in both training and inference.

Methods	FID ↓
ImageBART [21]	21.19
VQGAN [22]	15.78
IDDP [52]	12.30
VQ-D (T=100) [28]	11.89
Ours Sample-Inter (T=80)	11.96

while the *Sample-Inter* contrastive setting is more beneficial compared to *Step-Intra* for this image synthesis task. This empirical finding again validates our assumption regarding the contrastive settings in Sec. 3.3, where the *Sample-Inter* setting helps more with the instance-level synthesis quality. Notably, as shown in Fig. 4 (right), our contrastive diffusion method shows model convergence at about 60 diffusion steps, while the vanilla version converges at approximately 100 steps on CUB200 [78], which greatly increases the inference speed by 40%.

Class-Conditioned Image Synthesis. To demonstrate the robustness and generality of our proposed contrastive diffusion approach, we also perform the class-conditioned image generation on ImageNet [62]. We present the results comparisons using the FID score for generated images in Tab. 4, and show the implementation details and qualitative examples in the supplement.

5 Related Work

Diffusion Probabilistic Models (DPMs) [64] are first proposed to improve the tractability in machine learning, whose core design consists of a Markov chain of finite time steps in two opposite directions that transit between a data distribution and a non-informative noise. On the theoretical side, Ho *et al.* [32] introduce the Variational Lower Bound (VLB) objectives for original DPM. The model is further improved in [52] and obtains better log-likelihood scores. A large portion of following works seek to extend the diffusion models under a continuous-time setting [70, 71, 41, 69, 36, 77]. On the application side, DPMs have been successfully applied in various downstream tasks including image synthesis [32, 52, 16, 33, 35] and audio synthesis [42, 51, 45].

The research topic of multimodal learning, which incorporates data from various modalities such as audio, vision, and language has attracted much attention in recent years. General audio and visual learning works typically seek to investigate their correlations from the intrinsic synchronization nature [5, 43, 55, 56, 3], and then utilize them in various downstream audio-visual tasks such as audio-visual action recognition [40, 25], audio-visual event localization and parsing [74, 91, 82, 81], and audio-visual captioning [58, 80]. Works to generate music from visual or/and motion data have also been widely explored in recent years [23, 17, 1, 90]. For vision and language area, the text generation from visions are extensively explored in the image and video captioning task [92, 93, 2, 85, 79]. At the same time, works on image/video generation from text have also attracted much attention with recently released largescale models [57, 46, 61, 59].

6 Discussion

Conclusion. While DPMs have demonstrated remarkable potential, improving their training and inference efficiency while maintaining flexible and accurate results for conditional generation is an ongoing challenge, particularly for cross-modal tasks. Our Conditional Discrete Contrastive Diffusion (CDCD) loss addresses this by maximizing the mutual information between the conditioning input and the generated output. Our contrastive diffusion mechanisms and negative sampling methods

effectively incorporate this loss into DPM training. Extensive experiments on various cross-modal conditional generation tasks demonstrate the efficacy of our approach in bridging drastically differing domains. Exciting directions for future work include incorporating additional guidance into our contrastive learning process, and extending this work to DPMs operating in a continuous space.

Limitations and Social Impact. Though we significantly increase the training convergence and inference speed by reducing the number of diffusion steps required, the time and computation required for these DPMs is still fairly high. Finding further ways to improve efficiency is a direction we also seek to explore. As for broader social impact, as in other media generation works, there are possible malicious uses of such media to be addressed by oversight organizations and regulatory agencies.

References

- [1] Gunjan Aggarwal and Devi Parikh. Dance2music: Automatic dance-driven music generation. *arXiv preprint arXiv:2107.06252*, 2021.
- [2] Peter Anderson, Xiaodong He, Chris Buehler, Damien Teney, Mark Johnson, Stephen Gould, and Lei Zhang. Bottom-up and top-down attention for image captioning and visual question answering. In *CVPR*, 2018.
- [3] Relja Arandjelovic and Andrew Zisserman. Look, listen and learn. In *ICCV*, 2017.
- [4] Jacob Austin, Daniel Johnson, Jonathan Ho, Daniel Tarlow, and Rianne van den Berg. Structured denoising diffusion models in discrete state-spaces. In *NeurIPS*, 2021.
- [5] Yusuf Aytar, Carl Vondrick, and Antonio Torralba. Soundnet: Learning sound representations from unlabeled video. *NeurIPS*, 2016.
- [6] Philip Bachman, R Devon Hjelm, and William Buchwalter. Learning representations by maximizing mutual information across views. In *NeurIPS*, 2019.
- [7] Mohamed Ishmael Belghazi, Aristide Baratin, Sai Rajeshwar, Sherjil Ozair, Yoshua Bengio, Aaron Courville, and Devon Hjelm. Mutual information neural estimation. In *ICML*. PMLR, 2018.
- [8] Jean-Pierre Briot, Gaëtan Hadjeres, and François-David Pachet. *Deep learning techniques for music generation*, volume 1. Springer, 2020.
- [9] Z. Cao, G. Hidalgo Martinez, T. Simon, S. Wei, and Y. A. Sheikh. Openpose: Realtime multi-person 2d pose estimation using part affinity fields. *IEEE TPAMI*, 2019.
- [10] Zhe Cao, Tomas Simon, Shih-En Wei, and Yaser Sheikh. Realtime multi-person 2d pose estimation using part affinity fields. In *CVPR*, 2017.
- [11] Joao Carreira and Andrew Zisserman. Quo vadis, action recognition? a new model and the kinetics dataset. In *CVPR*, 2017.
- [12] Ting Chen, Simon Kornblith, Mohammad Norouzi, and Geoffrey Hinton. A simple framework for contrastive learning of visual representations. In *ICLR*, 2020.
- [13] Aiyu Cui, Daniel McKee, and Svetlana Lazebnik. Dressing in order: Recurrent person image generation for pose transfer, virtual try-on and outfit editing. In *CVPR*, 2021.
- [14] Jacob Devlin, Ming-Wei Chang, Kenton Lee, and Kristina Toutanova. Bert: Pre-training of deep bidirectional transformers for language understanding. *arXiv preprint arXiv:1810.04805*, 2018.
- [15] Prafulla Dhariwal, Heewoo Jun, Christine Payne, Jong Wook Kim, Alec Radford, and Ilya Sutskever. Jukebox: A generative model for music. *arXiv preprint arXiv:2005.00341*, 2020.
- [16] Prafulla Dhariwal and Alexander Nichol. Diffusion models beat gans on image synthesis. In *NeurIPS*, 2021.
- [17] Shangzhe Di, Zeren Jiang, Si Liu, Zhaokai Wang, Leyan Zhu, Zexin He, Hongming Liu, and Shuicheng Yan. Video background music generation with controllable music transformer. In *ACMMM*, 2021.
- [18] Hao-Wen Dong, Wen-Yi Hsiao, Li-Chia Yang, and Yi-Hsuan Yang. Musegan: Multi-track sequential generative adversarial networks for symbolic music generation and accompaniment. In *AAAI*, 2018.
- [19] Conor Durkan, Iain Murray, and George Papamakarios. On contrastive learning for likelihood-free inference. In *ICML*. PMLR, 2020.
- [20] Daniel PW Ellis. Beat tracking by dynamic programming. *Journal of New Music Research*, 2007.
- [21] Patrick Esser, Robin Rombach, Andreas Blattmann, and Bjorn Ommer. Imagebart: Bidirectional context with multinomial diffusion for autoregressive image synthesis. *NeurIPS*, 2021.
- [22] Patrick Esser, Robin Rombach, and Bjorn Ommer. Taming transformers for high-resolution image synthesis. In *CVPR*, 2021.
- [23] Chuang Gan, Deng Huang, Peihao Chen, Joshua B Tenenbaum, and Antonio Torralba. Foley music: Learning to generate music from videos. In *ECCV*, 2020.
- [24] Chuang Gan, Deng Huang, Hang Zhao, Joshua B Tenenbaum, and Antonio Torralba. Music gesture for visual sound separation. In *CVPR*, 2020.
- [25] Ruohan Gao, Tae-Hyun Oh, Kristen Grauman, and Lorenzo Torresani. Listen to look: Action recognition by previewing audio. In *CVPR*, 2020.
- [26] R. Gray. Vector quantization. *IEEE ASSP Magazine*, 1(2):4–29, 1984.

- [27] R.M. Gray and R.A. Olshen. Vector quantization and density estimation. In *Proceedings. Compression and Complexity of SEQUENCES 1997 (Cat. No.97TB100171)*, pages 172–193, 1997.
- [28] Shuyang Gu, Dong Chen, Jianmin Bao, Fang Wen, Bo Zhang, Dongdong Chen, Lu Yuan, and Baining Guo. Vector quantized diffusion model for text-to-image synthesis. *arXiv preprint arXiv:2111.14822*, 2021.
- [29] Kaiming He, Haoqi Fan, Yuxin Wu, Saining Xie, and Ross Girshick. Momentum contrast for unsupervised visual representation learning. In *CVPR*, 2020.
- [30] Jack Hessel, Ari Holtzman, Maxwell Forbes, Ronan Le Bras, and Yejin Choi. CLIPScore: a reference-free evaluation metric for image captioning. In *EMNLP*, 2021.
- [31] Martin Heusel, Hubert Ramsauer, Thomas Unterthiner, Bernhard Nessler, and Sepp Hochreiter. Gans trained by a two time-scale update rule converge to a local nash equilibrium. *NeurIPS*, 2017.
- [32] Jonathan Ho, Ajay Jain, and Pieter Abbeel. Denoising diffusion probabilistic models. In *NeurIPS*, 2020.
- [33] Jonathan Ho, Chitwan Saharia, William Chan, David J Fleet, Mohammad Norouzi, and Tim Salimans. Cascaded diffusion models for high fidelity image generation. *Journal of Machine Learning Research*, 2022.
- [34] Emiel Hooeboom, Didrik Nielsen, Priyank Jaini, Patrick Forré, and Max Welling. Argmax flows and multinomial diffusion: Towards non-autoregressive language models. *arXiv e-prints*, pages arXiv–2102, 2021.
- [35] Minghui Hu, Yujie Wang, Tat-Jen Cham, Jianfei Yang, and PN Suganthan. Global context with discrete diffusion in vector quantised modelling for image generation. *arXiv preprint arXiv:2112.01799*, 2021.
- [36] Chin-Wei Huang, Jae Hyun Lim, and Aaron C Courville. A variational perspective on diffusion-based generative models and score matching. In *NeurIPS*, 2021.
- [37] Cheng-Zhi Anna Huang, Ashish Vaswani, Jakob Uszkoreit, Noam Shazeer, Ian Simon, Curtis Hawthorne, Andrew M Dai, Matthew D Hoffman, Monica Dinulescu, and Douglas Eck. Music transformer: Generating music with long-term structure. In *ICLR*, 2019.
- [38] Shulei Ji, Jing Luo, and Xinyu Yang. A comprehensive survey on deep music generation: Multi-level representations, algorithms, evaluations, and future directions. *arXiv preprint arXiv:2011.06801*, 2020.
- [39] Will Kay, Joao Carreira, Karen Simonyan, Brian Zhang, Chloe Hillier, Sudheendra Vijayanarasimhan, Fabio Viola, Tim Green, Trevor Back, Paul Natsev, et al. The kinetics human action video dataset. *arXiv preprint arXiv:1705.06950*, 2017.
- [40] Evangelos Kazakos, Arsha Nagrani, Andrew Zisserman, and Dima Damen. Epic-fusion: Audio-visual temporal binding for egocentric action recognition. In *ICCV*, 2019.
- [41] Diederik P Kingma, Tim Salimans, Ben Poole, and Jonathan Ho. Variational diffusion models. In *NeurIPS*, 2021.
- [42] Zhifeng Kong, Wei Ping, Jiaji Huang, Kexin Zhao, and Bryan Catanzaro. Diffwave: A versatile diffusion model for audio synthesis. In *ICLR*, 2020.
- [43] Bruno Korbar, Du Tran, and Lorenzo Torresani. Cooperative learning of audio and video models from self-supervised synchronization. In *NeurIPS*, 2018.
- [44] Kundan Kumar, Rithesh Kumar, Thibault de Boissiere, Lucas Gestein, Wei Zhen Teoh, Jose Sotelo, Alexandre de Brébisson, Yoshua Bengio, and Aaron C Courville. Melgan: Generative adversarial networks for conditional waveform synthesis. In *NeurIPS*, 2019.
- [45] Junhyeok Lee and Seungu Han. Nu-wave: A diffusion probabilistic model for neural audio upsampling. *Proc. Interspeech 2021*, 2021.
- [46] Bowen Li, Xiaojuan Qi, Thomas Lukasiewicz, and Philip Torr. Controllable text-to-image generation. In *NeurIPS*, 2019.
- [47] Ruilong Li, Shan Yang, David A. Ross, and Angjoo Kanazawa. Ai choreographer: Music conditioned 3d dance generation with aist++. In *ICCV*, 2021.
- [48] Tsung-Yi Lin, Michael Maire, Serge Belongie, James Hays, Pietro Perona, Deva Ramanan, Piotr Dollár, and C Lawrence Zitnick. Microsoft coco: Common objects in context. In *ECCV*. Springer, 2014.
- [49] Matthew Loper, Naureen Mahmood, Javier Romero, Gerard Pons-Moll, and Michael J. Black. SMPL: A skinned multi-person linear model. *ACM Trans. Graphics (Proc. SIGGRAPH Asia)*, 34, 2015.

- [50] Ilya Loshchilov and Frank Hutter. Decoupled weight decay regularization. *arXiv preprint arXiv:1711.05101*, 2017.
- [51] Gautam Mittal, Jesse Engel, Curtis Hawthorne, and Ian Simon. Symbolic music generation with diffusion models. *arXiv preprint arXiv:2103.16091*, 2021.
- [52] Alexander Quinn Nichol and Prafulla Dhariwal. Improved denoising diffusion probabilistic models. In *International Conference on Machine Learning*. PMLR, 2021.
- [53] Aaron van den Oord, Yazhe Li, and Oriol Vinyals. Representation learning with contrastive predictive coding. *arXiv preprint arXiv:1807.03748*, 2018.
- [54] Aaron van den Oord, Oriol Vinyals, and Koray Kavukcuoglu. Neural discrete representation learning. In *NeurIPS*, 2017.
- [55] Andrew Owens and Alexei A Efros. Audio-visual scene analysis with self-supervised multisensory features. In *ECCV*, 2018.
- [56] Andrew Owens, Jiajun Wu, Josh H McDermott, William T Freeman, and Antonio Torralba. Ambient sound provides supervision for visual learning. In *ECCV*, 2016.
- [57] Alec Radford, Jong Wook Kim, Chris Hallacy, Aditya Ramesh, Gabriel Goh, Sandhini Agarwal, Girish Sastry, Amanda Askell, Pamela Mishkin, Jack Clark, et al. Learning transferable visual models from natural language supervision. In *ICML*. PMLR, 2021.
- [58] Tanzila Rahman, Bicheng Xu, and Leonid Sigal. Watch, listen and tell: Multi-modal weakly supervised dense event captioning. In *ICCV*, 2019.
- [59] Aditya Ramesh, Mikhail Pavlov, Gabriel Goh, Scott Gray, Chelsea Voss, Alec Radford, Mark Chen, and Ilya Sutskever. Zero-shot text-to-image generation. In *ICML*. PMLR, 2021.
- [60] Ali Razavi, Aaron van den Oord, and Oriol Vinyals. Generating diverse high-fidelity images with vq-vae-2. In *NeurIPS*, 2019.
- [61] Shulan Ruan, Yong Zhang, Kun Zhang, Yanbo Fan, Fan Tang, Qi Liu, and Enhong Chen. Dae-gan: Dynamic aspect-aware gan for text-to-image synthesis. In *ICCV*, 2021.
- [62] Olga Russakovsky, Jia Deng, Hao Su, Jonathan Krause, Sanjeev Satheesh, Sean Ma, Zhiheng Huang, Andrej Karpathy, Aditya Khosla, Michael Bernstein, et al. Imagenet large scale visual recognition challenge. *IJCV*, 2015.
- [63] Tim Sainburg, Marvin Thielk, and Timothy Q Gentner. Finding, visualizing, and quantifying latent structure across diverse animal vocal repertoires. *PLoS computational biology*, 16(10):e1008228, 2020.
- [64] Jascha Sohl-Dickstein, Eric Weiss, Niru Maheswaranathan, and Surya Ganguli. Deep unsupervised learning using nonequilibrium thermodynamics. In *ICML*. PMLR, 2015.
- [65] Jascha Sohl-Dickstein, Eric Weiss, Niru Maheswaranathan, and Surya Ganguli. Deep unsupervised learning using nonequilibrium thermodynamics. In *ICML*, 2015.
- [66] Jiaming Song and Stefano Ermon. Multi-label contrastive predictive coding. In *NeurIPS*, 2020.
- [67] Jiaming Song and Stefano Ermon. Understanding the limitations of variational mutual information estimators. In *ICLR*, 2020.
- [68] Jiaming Song, Chenlin Meng, and Stefano Ermon. Denoising diffusion implicit models. In *ICLR*, 2020.
- [69] Yang Song, Conor Durkan, Iain Murray, and Stefano Ermon. Maximum likelihood training of score-based diffusion models. In *NeurIPS*, 2021.
- [70] Yang Song and Stefano Ermon. Improved techniques for training score-based generative models. In *NeurIPS*, 2020.
- [71] Yang Song, Jascha Sohl-Dickstein, Diederik P Kingma, Abhishek Kumar, Stefano Ermon, and Ben Poole. Score-based generative modeling through stochastic differential equations. In *ICLR*, 2020.
- [72] Hongchen Tan, Xiuping Liu, Xin Li, Yi Zhang, and Baocai Yin. Semantics-enhanced adversarial nets for text-to-image synthesis. In *ICCV*, 2019.
- [73] Ming Tao, Hao Tang, Songsong Wu, Nicu Sebe, Xiao-Yuan Jing, Fei Wu, and Bingkun Bao. Df-gan: Deep fusion generative adversarial networks for text-to-image synthesis. *arXiv preprint arXiv:2008.05865*, 2020.
- [74] Yapeng Tian, Jing Shi, Bochen Li, Zhiyao Duan, and Chenliang Xu. Audio-visual event localization in unconstrained videos. In *ECCV*, 2018.
- [75] Hung-Yu Tseng, Matthew Fisher, Jingwan Lu, Yijun Li, Vladimir Kim, and Ming-Hsuan Yang. Modeling artistic workflows for image generation and editing. In *ECCV*. Springer, 2020.

- [76] Shuhei Tsuchida, Satoru Fukayama, Masahiro Hamasaki, and Masataka Goto. Aist dance video database: Multi-genre, multi-dancer, and multi-camera database for dance information processing. In *Proceedings of the 20th International Society for Music Information Retrieval Conference, (ISMIR)*, 2019.
- [77] Arash Vahdat, Karsten Kreis, and Jan Kautz. Score-based generative modeling in latent space. In *Advances in Neural Information Processing Systems*, 2021.
- [78] C. Wah, S. Branson, P. Welinder, P. Perona, and S. Belongie. The Caltech-UCSD Birds-200-2011 Dataset. Technical Report CNS-TR-2011-001, California Institute of Technology, 2011.
- [79] Liwei Wang, Alexander Schwing, and Svetlana Lazebnik. Diverse and accurate image description using a variational auto-encoder with an additive gaussian encoding space. In *NeurIPS*, 2017.
- [80] Xin Wang, Yuan-Fang Wang, and William Yang Wang. Watch, listen, and describe: Globally and locally aligned cross-modal attentions for video captioning. In *NAACL*, 2018.
- [81] Yu Wu and Yi Yang. Exploring heterogeneous clues for weakly-supervised audio-visual video parsing. In *CVPR*, 2021.
- [82] Yu Wu, Linchao Zhu, Yan Yan, and Yi Yang. Dual attention matching for audio-visual event localization. In *ICCV*, 2019.
- [83] Tao Xu, Pengchuan Zhang, Qiuyuan Huang, Han Zhang, Zhe Gan, Xiaolei Huang, and Xiaodong He. Attngan: Fine-grained text to image generation with attentional generative adversarial networks. In *CVPR*, 2018.
- [84] Zipeng Xu, Tianwei Lin, Hao Tang, Fu Li, Dongliang He, Nicu Sebe, Radu Timofte, Luc Van Gool, and Errui Ding. Predict, prevent, and evaluate: Disentangled text-driven image manipulation empowered by pre-trained vision-language model. *arXiv preprint arXiv:2111.13333*, 2021.
- [85] Quanzeng You, Hailin Jin, Zhaowen Wang, Chen Fang, and Jiebo Luo. Image captioning with semantic attention. In *CVPR*, 2016.
- [86] Han Zhang, Jing Yu Koh, Jason Baldridge, Honglak Lee, and Yinfei Yang. Cross-modal contrastive learning for text-to-image generation. In *CVPR*, 2021.
- [87] Han Zhang, Tao Xu, Hongsheng Li, Shaoting Zhang, Xiaogang Wang, Xiaolei Huang, and Dimitris N Metaxas. Stackgan: Text to photo-realistic image synthesis with stacked generative adversarial networks. In *CVPR*, 2017.
- [88] Han Zhang, Tao Xu, Hongsheng Li, Shaoting Zhang, Xiaogang Wang, Xiaolei Huang, and Dimitris N Metaxas. Stackgan++: Realistic image synthesis with stacked generative adversarial networks. *IEEE TPAMI*, 2018.
- [89] Minfeng Zhu, Pingbo Pan, Wei Chen, and Yi Yang. Dm-gan: Dynamic memory generative adversarial networks for text-to-image synthesis. In *CVPR*, 2019.
- [90] Ye Zhu, Kyle Olszewski, Yu Wu, Panos Achlioptas, Menglei Chai, Yan Yan, and Sergey Tulyakov. Quantized gan for complex music generation from dance videos. *arXiv preprint arXiv:2204.00604*, 2022.
- [91] Ye Zhu, Yu Wu, Hugo Latapie, Yi Yang, and Yan Yan. Learning audio-visual correlations from variational cross-modal generation. In *ICCAPS*, 2021.
- [92] Ye Zhu, Yu Wu, Yi Yang, and Yan Yan. Describing unseen videos via multi-modal cooperative dialog agents. In *ECCV*, 2020.
- [93] Ye Zhu, Yu Wu, Yi Yang, and Yan Yan. Saying the unseen: Video descriptions via dialog agents. In *TPAMI*, 2021.

A More Qualitative Results

A.1 Generated Music Samples

For qualitative samples of synthesized dance music sequences, please refer to our project page with music samples. In addition to the generated music samples on AIST++ [76, 47] and TikTok Dance-Music Dataset [90], we also include some qualitative samples obtained with the music editing operations based on the dance-music genre annotations from AIST++. Specifically, we edit the original paired motion conditioning input with a different dance-music genre using a different dance choreographer.

Discussion on Musical Representations and Audio Quality. It is worth noting that we only compare the overall audio quality with that of D2M-GAN [90]. This is due to the nature of the different musical representations in the literature of deep-learning based music generation [23, 18, 37, 24, 1]. There are mainly two categories for adopted musical representations in previous works: pre-defined symbolic and learning-based representations [38, 8]. For the former symbolic music representation, typical options include 1D piano-roll and 2D MIDI-based representations. While these works benefit from the pre-defined music synthesizers and produce music that does not include raw audio noise, the main limitation is that such representations are usually limited to a single specific instrument, which hinders their flexibility to be applied in wider and more complex scenarios such as dance videos. In contrast, the learning-based music representations (*i.e.* musical VQ in our case) rely on well-trained music synthesizers as decoders, but can be used as a unified representation for various musical sounds, *e.g.* instruments or voices. However, the training of such music encoders and decoders for high-quality audio signals itself remains a challenging problem. Specifically, high-quality audio is a form of high-dimensional data with an extremely large sampling rate, even compared to high-resolution images. For example, the sampling rate for CD-quality audio signals is 44.1 kHz, resulting in 2,646,000 data points for a one-minute musical piece. To this end, existing deep learning based works [15, 44] for music generation employ methods to reduce the number of dimensions, *e.g.* by introducing hop lengths and a smaller sampling rate. These operations help to make music learning and generation more computationally tractable, but also introduce additional noise in the synthesized audio signals.

In this work, we adopt the pre-trained JukeBox model [15] as our music encoder and decoder for the musical VQ representation. The adopted model has a hop length of 128, which corresponds to the top-level model from their original work [15]. Jukebox employs 3 models: top-, middle-, and bottom-level, with both audio quality and required computation increasing from the first to the last model. While they allow for high-quality audio reconstruction (from the bottom-level model, with a hop length of 8), it requires much more time and computation not only for training but also for the final inference, *e.g.* 3 hours to generate a 20-second musical sequence. As the synthesized music from the top-level model includes some audible noise, we apply a noise reduction operation [63]. However, the overall audio quality is not a primary factor that we specifically address in this work on cross-modal conditioning and generation, as it largely depends on the specific music encoder and decoder that are employed. This explains why we report similar MOS scores in terms of the general audio quality.

A.2 Synthesized Images

We present more qualitative examples for text-to-image synthesis and class-conditioned image synthesis in Fig. 5, Fig. 6, and Fig. 7.

B Detailed Proof and Training

B.1 Lower Bound of CDCD Loss

We show that the proposed *CDCD* loss has a lower bound related to the mutual information and the number of negative samples N . The derivations below are similar to those from [53]:

$$\mathcal{L}_{\text{CDCD}} = \mathbb{E}_Z \left[-\log \frac{\frac{p_\theta(z_0|c)}{p_\theta(z_0)}}{\frac{p_\theta(z_0|c)}{p_\theta(z_0)} + \sum_{z^j \in Z'} \frac{p_\theta(z_0^j|c)}{p_\theta(z_0^j)}} \right] \quad (6a)$$

$$= \mathbb{E}_Z \log \left[1 + \frac{p_\theta(z_0)}{p_\theta(z_0|c)} \sum_{z^j \in Z'} \frac{p_\theta(z_0^j|c)}{p_\theta(z_0^j)} \right] \quad (6b)$$

$$\approx \mathbb{E}_Z \log \left[1 + N \frac{p_\theta(z_0)}{p_\theta(z_0|c)} \mathbb{E}_{Z'} \left[\frac{p_\theta(z_0^j|c)}{p_\theta(z_0^j)} \right] \right] \quad (6c)$$

$$= \mathbb{E}_Z \log \left[1 + N \frac{p_\theta(z_0)}{p_\theta(z_0|c)} \right] \quad (6d)$$

$$\geq \mathbb{E}_Z \log \left[N \frac{p_\theta(z_0)}{p_\theta(z_0|c)} \right] \quad (6e)$$

$$= \log(N) - I(z_0, c). \quad (6f)$$

B.2 Step-Wise and Sample-Wise Contrastive Diffusion

We show the full derivation for the step-wise parallel contrastive diffusion loss:

$$\mathcal{L}_{\text{CDCD-Step}} \approx \mathbb{E}_Z \log \left[1 + \frac{p_\theta(z_{0:T})}{p_\theta(z_{0:T}|c)} N \mathbb{E}_{Z'} \left[\frac{p_\theta(z_{0:T}^j|c)}{p_\theta(z_{0:T}^j)} \right] \right] \quad (7a)$$

$$\approx \mathbb{E}_Z \mathbb{E}_q \log \left[\frac{p_\theta(z_{0:T})}{q(z_{1:T}|z_0)} N \frac{q(z_{1:T}|z_0)}{p_\theta(z_{0:T}|c)} \right] \quad (7b)$$

$$\approx \mathbb{E}_q \left[-\log \frac{p_\theta(z_{0:T})}{q(z_{1:T}|z_0)} \right] - N \mathbb{E}_{Z'} \mathbb{E}_q \left[-\log \frac{p_\theta(z_{0:T}|c)}{q(z_{1:T}|z_0)} \right] \quad (7c)$$

$$\approx \mathcal{L}_{\text{vb}}(z) - \sum_{z^j \in Z'} \mathcal{L}_{\text{vb}}(z^j, c). \quad (7d)$$

For the sample-wise auxiliary contrastive diffusion, the loss can be derived as follows:

$$\mathcal{L}_{\text{CDCD-Sample}} \approx \mathbb{E}_Z \log \left[1 + \frac{p_\theta(z_0)}{p_\theta(z_0|c)} N \mathbb{E}_{Z'} \left[\frac{p_\theta(z_0^j|c)}{p_\theta(z_0^j)} \right] \right] \quad (8a)$$

$$\approx \mathbb{E}_Z \mathbb{E}_q \log \left[\frac{p_\theta(z_0)}{q(z_{1:T}|z_0)} N \frac{q(z_{1:T}|z_0)}{p_\theta(z_0|c)} \right] \quad (8b)$$

$$\approx \mathbb{E}_q \left[-\log \frac{p_\theta(z_{0:T})}{q(z_{1:T}|z_0)} \right] - N \mathbb{E}_{Z'} \mathbb{E}_q \left[-\log \frac{p_\theta(z_{0:T}|c)}{q(z_{1:T}|z_0)} \right] \quad (8c)$$

$$\approx \mathbb{E}_q \left[-\log p_\theta(z_0|z_t) \right] - \sum_{z^j \in Z'} \mathbb{E}_q \left[-\log p_\theta(z_0^j|z_t, c) \right]. \quad (8d)$$

Algorithm 1 Conditional Discrete Contrastive Diffusion Training. The referenced equations can be found in the main paper.

Input: Initial network parameters θ , contrastive loss weight λ , learning rate η , number of negative samples N , total diffusion steps T , conditioning information c , contrastive mode $m \in \{\text{Step}, \text{Sample}\}$.

```

1: for each training iteration do
2:    $t \sim \text{Uniform}(\{1, 2, \dots, T\})$ 
3:    $z_t \leftarrow \text{Sample from } q(z_t | z_{t-1})$ 
4:    $\mathcal{L}_{\text{vb}} \leftarrow \sum_{i=1, \dots, t} \mathcal{L}_i \triangleright \text{Eq. 1}$ 
5:   if  $m == \text{Step}$  then
6:     for  $j = 1, \dots, N$  do
7:        $z_t^j \leftarrow \text{Sample from } q(z_t^j | z_{t-1}^j, c) \triangleright \text{from negative variables in previous steps}$ 
8:     end for
9:      $\mathcal{L}_{\text{CDDCD}} = -\frac{1}{N} \sum \mathcal{L}_{\text{vb}}^j \triangleright \text{Eq. 3}$ 
10:  else if  $m == \text{Sample}$  then
11:    for  $j = 1, \dots, N$  do
12:       $z_t \leftarrow \text{Sample from } q(z_t | z_0^j, c) \triangleright \text{from negative variables in step 0}$ 
13:    end for
14:     $\mathcal{L}_{\text{CDDCD}} = -\frac{1}{N} \sum \mathcal{L}_{z_0}^j \triangleright \text{Eq. 4}$ 
15:  end if
16:   $\mathcal{L} \leftarrow \mathcal{L}_{\text{vb}} + \lambda \mathcal{L}_{\text{CDDCD}} \triangleright \text{Eq. 5}$ 
17:   $\theta \leftarrow \theta - \eta \nabla_{\theta} \mathcal{L}$ 
18: end for

```

B.3 Conventional Variational Loss

The conventional variational loss \mathcal{L}_{vb} is derived as follows [64]:

$$\begin{aligned}
\mathcal{L}_{\text{vb}}(x) &= \mathbb{E}_q[-\log \frac{p_{\theta}(x_{0:T})}{q(x_{1:T}|x_0)}] \\
&= \mathbb{E}_q[-\log p(x_T) - \sum_{t>1} \log \frac{p_{\theta}(x_{t-1}|x_t)}{q(x_t|x_{t-1})} - \log \frac{p_{\theta}(x_0|x_1)}{q(x_1|x_0)}] \\
&= \mathbb{E}_q[-\log p(x_T) - \sum_{t>1} \log \frac{p_{\theta}(x_{t-1}|x_t)}{q(x_{t-1}|x_t, x_0)} \cdot \frac{q(x_{t-1}|x_0)}{q(x_t|x_0)} - \log \frac{p_{\theta}(x_0|x_1)}{q(x_1|x_0)}] \\
&= \mathbb{E}_q[-\log \frac{p(x_T)}{q(x_T|x_0)} - \sum_{t>1} \log \frac{p_{\theta}(x_{t-1}|x_t)}{q(x_{t-1}|x_t, x_0)} - \log p_{\theta}(x_0|x_1)] \\
&= \mathbb{E}_q[D_{\text{KL}}(q(x_T|x_0)||p(x_T)) + \sum_{t>1} D_{\text{KL}}(q(x_{t-1}|x_t, x_0)||p_{\theta}(x_{t-1}|x_t)) - \log p_{\theta}(x_0|x_1)].
\end{aligned} \tag{9}$$

B.4 Conditional Discrete Contrastive Diffusion Training

The training process for the proposed contrastive diffusion is explained in Algo. 1.

C Additional Experimental Details and Analysis

C.1 Dance-to-Music Task

Implementation. The sampling rate for all audio signals is 22.5 kHz in our experiments. We use 2-second music samples as in [90] for our main experiments, resulting in 44,100 audio data points for each raw music sequence. For the Music VQ-VAE, we fine-tuned Jukebox [15] on our data to leverage its pre-learned codebook from a large-scale music dataset (approximately 1.2 million songs). The codebook size K is 2048, with a token dimension $d_z = 128$, and the hop-length L is 128 in our default experimental setting. For the motion module, we deploy a backbone stacked with convolutional layers and residual blocks. The dimension size of the embedding we use for music conditioning is 1024. For the visual module, we extract I3D features [11] using a model pre-trained on Kinetics [39] as the visual conditioning information, with a dimension size of 2048. In the

Table 5: Complete quantitative evaluation results for the dance-to-music generation task on the AIST++ dataset. We report the mean and standard deviations of our contrastive diffusion for three inference tests.

Musical features	Rhythms	Rhythms	Genre	Coherence	Quality
Metrics	Coverage \uparrow	Hit \uparrow	Accuracy \uparrow	MOS \uparrow	MOS \uparrow
GT Music	100	100	88.5	4.7	4.8
Foley [23]	74.1	69.4	8.1	2.9	-
Dance2Music [1]	83.5	82.4	7.0	3.0	-
CMT [17]	85.5	83.5	11.6	3.0	-
D2M-GAN [90]	88.2	84.7	24.4	3.3	3.4
Ours Vanilla	89.0 \pm 1.1	83.8 \pm 1.5	25.3 \pm 0.8	3.3	3.6
Ours Step-Intra	93.9 \pm 1.2	90.7 \pm 1.5	25.8 \pm 0.6	3.6	3.5
Ours Step-Inter	92.4 \pm 1.0	88.9 \pm 1.7	24.3 \pm 0.7	3.4	3.5
Ours Sample-Intra	91.5 \pm 1.7	84.6 \pm 1.6	26.0 \pm 0.8	3.5	3.6
Ours Sample-Inter	91.8 \pm 1.6	86.9 \pm 1.4	27.2 \pm 0.5	3.6	3.6

implementation of our contrastive diffusion model, we adopt a transformer-based backbone to learn the denoising network p_θ . It includes 19 transformer blocks, in which each block consists of full-attention, cross-attention and a feed-forward network, and the channel size for each block is 1024. We set the initial weight for the contrastive loss as $\lambda = 5e - 5$. The numbers of intra- and inter-negative samples for each GT music sample are both 10. The AdamW [50] optimizer with $\beta_1 = 0.9$ and $\beta_2 = 0.96$ is deployed in our training, with a learning rate of $4.5e - 4$. We also employ an adaptive weight for the denoising loss weight by gradually decreasing the weight as the diffusion step increases and approaches the end of the chain. The visual module, motion module, and the contrastive diffusion model are jointly optimized.

Other than the aforementioned implementation details, we also include the mask token technique that bears resemblance to those used in language modelling [14] and text-to-image synthesis [28] for our dance-to-music generation task. We adopt a truncation rate of 0.86 in our inference.

MOS Evaluation Test. We asked a total of 32 participants to participate in our subjective Mean Opinion Scores (MOS) music evaluations [90, 44], among which 11 of them are female, while the rest are male. For the dance-music coherence test, we fuse the generated music samples with the GT videos as post-processing. We then asked each evaluator to rate 20 generated videos with a score of 1 (least coherent) to 5 (most coherent) after watching the processed video clip. Specifically, the participants are asked to pay more attention to the dance-music coherence in terms of the dance moves corresponding to the music genre and rhythm, rather than the overall music quality, with reference to the GT video clips with the original music. As for the overall quality evaluations, we only play the audio tracks without the video frames to each evaluator. As before, they are asked to rate the overall music quality with a score of 1 (worst audio quality) to 5 (best audio quality).

Training Cost. For the dance2music task experiments on the AIST++ dataset, we use 4 NVIDIA RTX A5000 GPUs, and train the model for approximately 2 days. For the same task on the TikTok dance-music dataset, the training takes approximately 1.5 days on the same hardware.

Complete Results for Contrastive Settings. As discussed in our main paper, there are four possible combinations for contrastive settings given different contrastive diffusion mechanisms and negative sampling methods. Here, we include complete quantitative scores for different contrastive settings in Tab. 5. We observe that all the four contrastive settings, including the *Step-Inter* and *Sample-Intra* settings that are not reported in our main paper, help to improve the performance. As we noted, amongst all the settings, *Step-Intra* and *Sample-Inter* are more reasonable and yield larger improvements for intra-sample data attributes (*i.e.* beats scores) and instance-level features (*i.e.* genre accuracy scores).

Ablation on Music Length. Although we use 2-second musical sequences in the main experiments to make for consistent and fair comparisons with [90], our framework can also synthesize longer musical sequences. In the supplementary, we show our generated music sequences in 6-seconds. The quantitative evaluations in terms of different musical sequence lengths are presented Tab. 6, where we show better performance when synthesizing longer musical sequences.

Table 6: Ablation results for different music lengths on the AIST++ dataset.

Length	Methods	Beats Coverage \uparrow	Beats Hit \uparrow	Genre Acc. \uparrow
2s	D2M-GAN [90]	88.2	84.7	24.4
	Ours Vanilla	89.0	83.8	25.3
	Ours Step-Intra	93.9	90.7	25.8
	Ours Sample-Inter	91.8	86.9	27.2
4s	D2M-GAN [90]	87.1	83.0	23.3
	Ours Vanilla	86.2	81.8	24.6
	Ours Step-Intra	93.1	86.4	25.3
	Ours Sample-Inter	91.4	83.9	26.1
6s	D2M-GAN [90]	-	-	-
	Ours Vanilla	84.8	81.1	22.7
	Ours Step-Intra	87.9	83.2	22.9
	Ours Sample-Inter	86.3	81.6	23.0

C.2 Text-to-Image Task

Implementation. For the text-to-image generation task, we adopt VQ-GAN [22] as the discrete encoder and decoder. The codebook size K is 2886, with a token dimension $d_z = 256$. VQ-GAN converts a 256×256 resolution image to 32×32 discrete tokens. For the textual conditioning, we employ the pre-trained CLIP [57] model to encode the given textual descriptions. The denoising diffusion model p_θ has 18 transformer blocks and a channel size of 192, which is a similar model scale to the small version of VQ-Diffusion [28]. We use $\lambda = 5e - 5$ as the contrastive loss weight. Similar to the dance-to-music task, we also use the adaptive weight that changes within the diffusion stages. We keep the same truncation rate of 0.86 as in our dance-to-music experiment and in [28]. Unlike in the dance-to-music experiments, where we jointly learn the conditioning encoders, both the VQ-GAN and CLIP models are fixed during the contrastive diffusion training.

Training Cost. For the text2image task experiments on the CUB200 dataset, the training takes approximately 5 days using 4 NVIDIA RTX A5000 GPUs. For the same experiments on the MSCOCO dataset, we run the experiments on Amazon Web Services (AWS) using 8 NVIDIA Tesla V100 GPUs. This task required 10 days of training.

C.3 Class-Conditioned Image Synthesis Task

Implementation. For the class-conditioned image synthesis, we also adopt the pre-trained VQ-GAN [22] as the discrete encoder and decoder. We replace the conditioning encoder with class embedding optimized during the contrastive diffusion training. The size of the conditional embedding is 512. Other parameters and techniques remain the same, as in the text-to-image task.

Training Cost. For the class-conditioned experiments on the ImageNet, we use 8 NVIDIA Tesla V100 GPUs running on AWS. This task required 15 days of training.



Figure 5: More qualitative results from our text-to-image experiments on CUB200 dataset. We show examples of the text input (left column), the synthesized images from our contrastive diffusion model with 80 diffusion steps and a FID score of 12.61 (middle column), and the output from existing method [28] with 100 diffusion steps and a FID score 12.97.

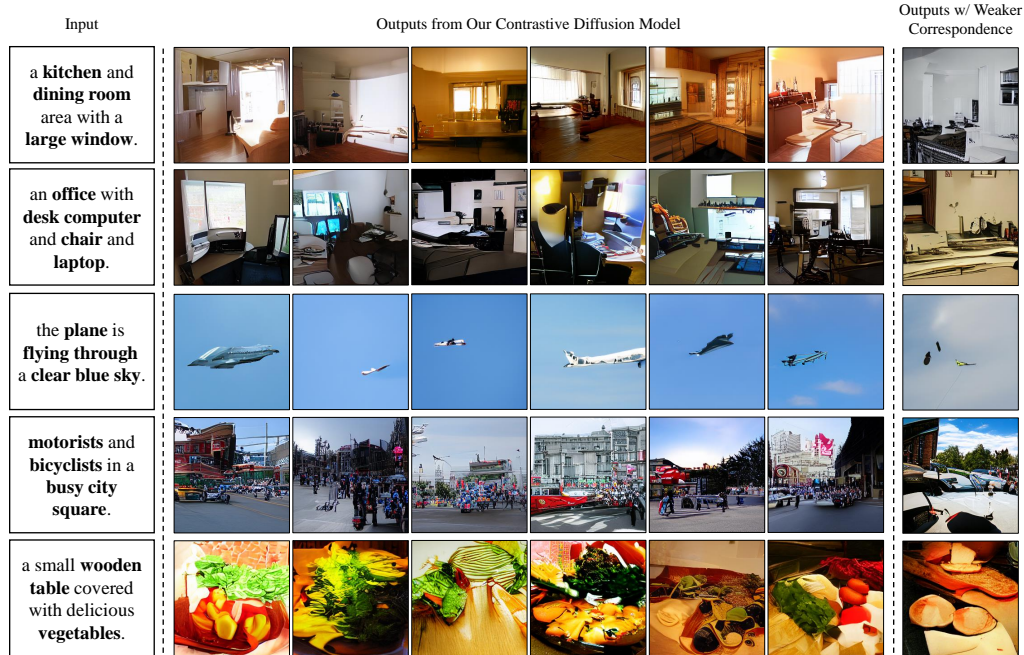


Figure 6: More qualitative results from our text-to-image experiments on COCO dataset. We show examples of the text input (left column), the synthesized images from our contrastive diffusion model with 80 diffusion steps and a FID score of 28.76 (middle column), and the output from existing method [28] with 100 diffusion steps and a FID score 30.17.

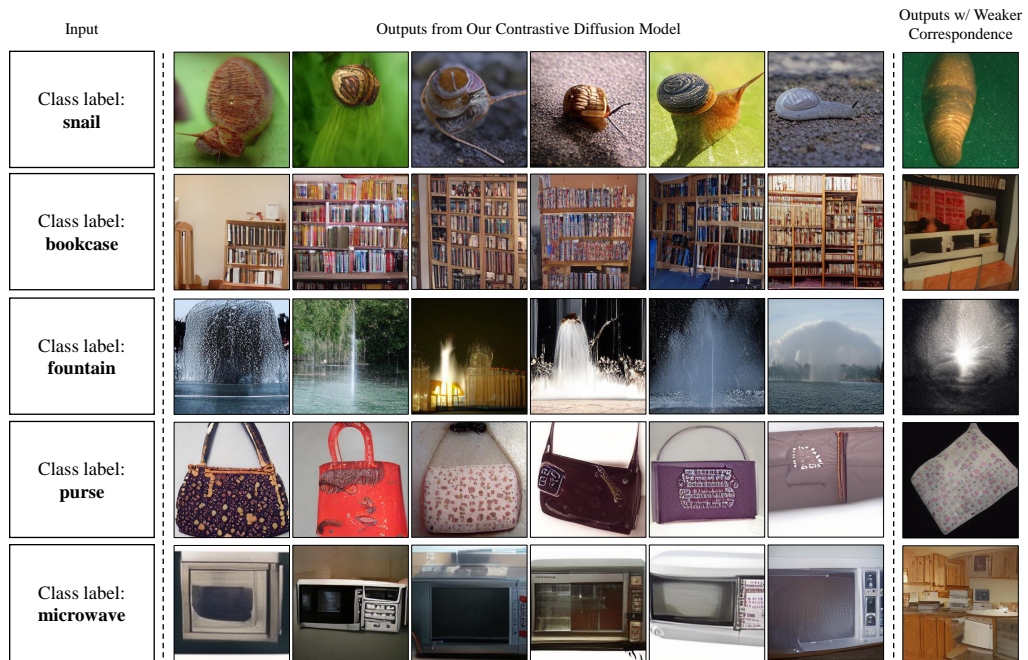


Figure 7: More qualitative results from our class-conditioned image synthesis experiments on ImageNet. We show examples of the text input (left column), the synthesized images from our contrastive diffusion model with 80 diffusion steps and a FID score of 12.41 (middle column), and the output from existing method [28] with 100 diffusion steps and a FID score 11.89.